Effects of Ni doping on structural, magnetic and catalytic properties of copper ferrite

Zbigniew S. Piskuła[1*], Jolanta Darul[1], Maria Szafran[1], Tomasz Toliński[2], Waldemar Nowicki[1]

[1]Faculty of Chemistry, Adam Mickiewicz University, Poznań, Poland

[2]Institute of Molecular Physics, Polish Academy of Sciences, Poznań, Poland

Abstract

The aim of this work was to obtain information about the influence of small quantities of Ni^{2+} ion on the structural and magnetic properties of the tetragonally distorted of $Cu_{1-x}Ni_xFe_2O_4$ series (with x = 0.00, 0.05, 0.1, and 0.15 respectively). The tested ferrite system was synthesized by combustion of citrate-nitrate precursors. The synchrotron X-ray diffraction measurements determined the phase transition temperatures (tetragonal → cubic) of all samples. The change of structures under the influence of temperature shows a phase transition in the range of 390 – 400 °C for x = 0.00, 330 – 370 °C for x = 0.05, 210 – 330 °C for x = 0.1 and 140 – 210 °C for x = 0.15, respectively. The initial phase transition temperature decreases linearly with the decreasing *c/a* ratio of the crystallographic lattice parameters for the $Cu_{1-x}Ni_xFe_2O_4$ oxides. Hysteresis measurements were made to determine the saturation magnetization (M_S) and coercive field ($\mu_0 H_c$) of the samples. The values of magnetic moments at room temperature determined from magnetization measurements are very similar to those obtained from theoretical x-ray diffraction calculations. Magnetic moment values per formula unit are estimated to range from 1.16 μB to 1.5 μB. It was found that the catalytic activity of N_2O decomposition of samples increases with increasing nickel content.

Keywords: Cuproferrites**,** Synchrotron X-ray diffraction, Phase transition, Magnetization, Jahn-Teller effect, N_2O decomposition.

*) Corresponding author: Zbigniew S. Piskuła

Faculty of Chemistry, Adam Mickiewicz University, Uniwersytetu Poznańskiego 8, 61-614, Poznań, Poland

Tel./Fax: +48618291803

E-mail: zpiskula@amu.edu.pl

1. Introduction

Polycrystalline copper ferrites are one of the most important ferrites, they are soft magnetic materials with a good potential for novel applications as spintronics, drug delivery, and data storage [1-4]. $CuFe_2O_4$ crystallizes in cubic or in tetragonal symmetry depending on the cation distribution in the two different crystallographic sites (A- tetrahedral and B- octahedral) of the spinel structure. The cation distribution in this oxide can be presented by the formula: $(Cu_x^{2+}Fe_{1-x}^{3+})_A[Cu_{1-x}^{2+}Fe_{1+x}^{3+}]_BO_4$. The parameter of inversion x = 0 for inversion spinels, and x = 1, when the spinel is normal. The structure of the $CuFe_2O_4$ can be controlled by annealing and cooling rates during the process of compound preparation. Copper ferrite quenched at temperatures above 800 ^oC has a cubic structure, while slowly cooled it has a tetragonally deformed spinel structure [5-6]. This material is ferrimagnetic with a Curie temperature T_c = 770 K [6]. The introduction of magnetic and nonmagnetic ions into tetrahedral (A) and octahedral (B) spinel sites generates different magnetic order, and this is mainly due to modifications in the intersublattice space (A - O - B) and intersublattice space (A - O - A) and (B - O - B) exchange interactions. Structural and magnetic properties of ferrites are strictly guided by the cation distribution in their specified crystallographic sites. The characteristic properties of copper ferrites can be improved by combining other metallic ions in their chemical structure. Metal combination with ferrite can produce new substances with interesting properties. Many researchers have modified copper ferrite and obtained new materials with completely different structural, thermal, electrical, magnetic and catalytic properties [7-9].

The effect of nickel ion substitution for copper on structural, magnetic and catalytic activity properties of $CuFe_2O_4$ ferrite is reported. The impact of replacing Cu ions by Ni on the structural parameters and magnetic properties of the system was investigated utilizing synchrotron X-ray diffraction and magnetic measurements. Catalytic measurements of N_2O decomposition in $Cu_{1-x}Ni_xFe_2O_4$ systems were carried out depending on the nickel content in the sample.

2. Synthesis and experimental methods

A series of ferrite samples of the chemical composition $Cu_{1-x}Ni_xFe_2O_4$ (x = 0.0; 0.05; 0.1 and 0.15) prepared by a combustion method using citrate-nitrate precursors. All reagents were of high analytical grade and were obtained from Sigma Aldrich and Merck Chemical. The stoichiometric quantities of starting materials, viz., $Cu(NO_3)_2 \cdot 6H_2O$, $Ni(NO_3)_2 \cdot 6H_2O$,

$Fe(NO_3)_3 \cdot 9H_2O$, (Merck) and $C_6H_8O_7 \cdot H_2O$, were dissolved in distilled water. The mixed citrate-nitrate solution was heated at 120 °C, with continuous stirring. After the evaporation of excess of water, a highly viscous gel was obtained. Ultimately, the powder was sintered in air at different temperatures (300, 600, 900 °C) for 4h. After heating, the preparations were cooled slowly to room temperature.

The compounds formation and crystallinity of the materials were identified by XRD patterns, which were recorded on a computerized TUR_M61 (HZG-3) diffractometer, employing Co Kα radiation. Finally, investigations on the temperature phase transition for product formed as a result of slow cooling of $Cu_{1-x}Ni_xFe_2O_4$ samples were carried out at the synchrotron beamline B2 at Hasylab (Desy, Hamburg). The diffractometer was equipped with capillary furnace (STOE) and the on-site readable image-plate detector OBI. The polycrystalline samples placed in quartz capillaries of diameter 0.3 mm were heated and cooled at the temperature range from RT to 500 °C. The wavelength, determined by calibration using a NIST silicon standard, was 0.688268 Å. Analysis of the XRD data was undertaken with a full-pattern fitting procedure based on the Rietveld method. Structure refinement was performed using *FullProf* program [10].

The studied ferrite samples of the chemical composition $Cu_{1-x}Ni_xFe_2O_4$ are characterized by magnetic ordering temperature of the order of 800 K, depending on the composition used. Therefore, to derive magnetic parameters, measurements in a wide temperatures range were carried out. Up to 400 K vibrating sample (VSM) option of the Physical Property Measurement System (PPMS), Quantum Design, was used. The magnetic characterization included magnetic susceptibility in the zero field-cooled (ZFC) mode (magnetic field switched on after cooling the sample down and then data acquisition during heating) and in the field-cooled (FC) mode (measurement during cooling down in a magnetic field, just after the ZFC procedure). For these ZFC-FC measurements magnetic field was set to 1 kOe. For temperatures from RT up to 850 K we employed a home-made magnetic susceptometer working based on the compensation method.

Textural parameters were obtained from the nitrogen adsorption–desorption isotherms at 77 K, and were recorded performed using Micromeritics ASAP V2.00D analyser. The specific surface area was calculated using multipoint BET analysis and the pore sizes were measured by the Barrett–Joyner–Halenda (BJH) method of desorption.

Catalytic activity was carried out by the TPR (temperature programmed reaction) method. A 100 mg sample was placed in a quartz reactor, the system was conditioned at 973 K for 2 h in an argon atmosphere with a gas flow of 50 cm^3/min. A gas mixture of 5000 ppm N_2O in Ar

was fed at the constant rate of 50 cm^3/min (weight hourly space velocity, WHSV = 30000 ml g^{-1} h^{-1}) via a set of mass flow controllers to the quartz microreactor placed in an electric oven. The PID controller was used to regulate the heating power and control the temperature. Measurements were made in the range of 473 - 973 K. The results were performed in a gas analyzer Pfeiffer ThermoStar model GDS301T2 using QMA200M analyzer. The N_2O conversion was calculated according to equation (1):

$$\%N_2O_{conv} = \frac{N_2O_{total} - N_2O_{\text{residual}}}{N_2O_{total}} \times 100 \quad (1)$$

the CRSA (conversion rate per square meter of surface area) was calculated from equation (2):

$$CRSA = \frac{\left[\frac{N_2O_{total} - N_2O_{residual}}{N_2O_{total}}\right]}{m_s \cdot S_{BET}} \quad (2)$$

3. Structural properties

The X-ray powder diffraction (XRD) patterns registered with using Co radiation of the $Cu_{1-x}Ni_xFe_2O_4$ compositions calcined at 900 °C have been shown in **Figure 1**. As shown in the formulas, all peaks confirm the formation of a single-phase system with a tetragonal copper ferrite structure type (JCPDS no. 34-0425) without additional peaks corresponding to any other phase [11]. It is well known that slow cooled $CuFe_2O_4$ from high temperatures has tetragonally deformed spinel structure at room temperature [12-15]. The crystal structure diagram of the $CuFe_2O_4$ sample is shown in **Figure 2**. Copper ferrite is an inverse spinel in which half of the Fe^{3+} ions occupy the tetrahedral sites (A sites) and the rest Fe^{3+} ions and all Cu^{2+} ions preferentially fill the octahedral sites [B sites], thus the compound can be presented by the formula: (Fe)[CuFe]O_4. The Cu^{2+} ions occur octahedral B sites and this causes the tetragonal distortion due to the cooperative Jahn-Teller effect [15]. The Jahn–Teller effect at Cu^{2+} is attributable to increase the distance of Cu–O bonds along the *c* axis, i.e. a distortion of the CuO_6 octahedron (**Fig. 2**). The structural parameters of the sample series are presented in **Table 1**. To provide a convenient comparison between cubic and tetragonal structures, the unit cell parameter in *a* tetragonal lattice is multiplied by $\sqrt{2}$. From **Table 1** shows that the volume, *c* parameter, *c*/*a*, and the Cu-O bond distance along the c-axis linearly decrease with the increase Ni^{2+} content in $Cu_{1-x}Ni_xFe_2O_4$ system. But, with increase Ni^{2+} content, the value of lattice parameter *a* and the Cu-O bond distance along the a-b plane linearly increase in

observed structures. It is well known, that Ni^{2+} occupies only the B-sites [16], based on these facts substitution of Cu^{2+} by Ni^{2+} leads to decrease of the *c/a* ratio, the resulting decrease copper ions in the octahedral sites gives rise to a less distorted structure. At the same time, the unit cell volume values decrease with increasing nickel concentration in the sample series because the ionic radius of Ni^{2+} is smaller than the ionic radius of Cu^{2+} [17].

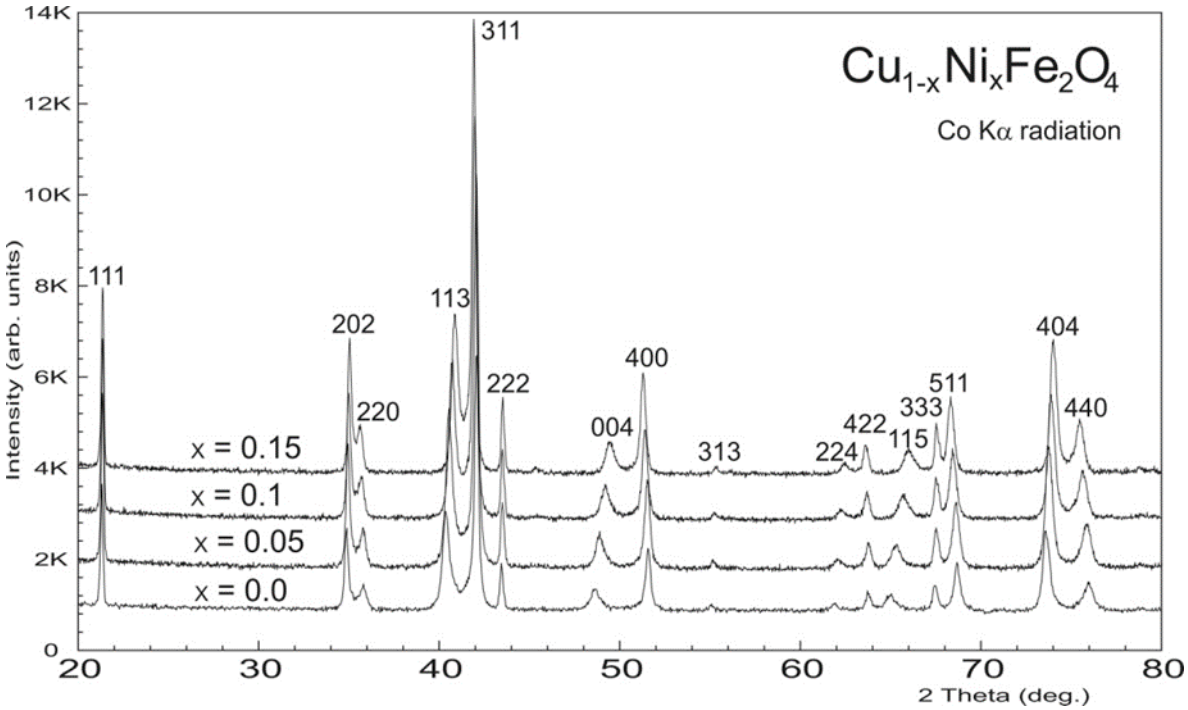

Figure 1. X-ray powder diffraction patterns of $Cu_{1-x}Ni_xFe_2O_4$ samples. The indices *hkl* correspond to the tetragonal spinel unit cell.

Table 1. Structural parameters for $Cu_{1-x}Ni_xFe_2O_4$ samples with tetragonal spinel unit cell at the room temperature.

Composition (x)	***a* [Å]** ($a = a_T \cdot \sqrt{2}$)	***c* [Å]**	***V* [Å^3]**	***c/a***	****Cu-O^c* [Å]**	****Cu-O^{a-b}* [Å]**
0.00	8.2255(3)	8.686(2)	591.55(05)	1.056	2.174	1.992
0.05	8.2429(6)	8.653(4)	587.93(10)	1.049	2.165	1.996
0.10	8.2584(7)	8.603(7)	586.73(06)	1.042	2.153	1.999
0.15	8.2727(4)	8.561(8)	585.89(08)	1.035	2.142	2.003

* Bond distances along the *c*-axis, and along the *a*-*b* plane.

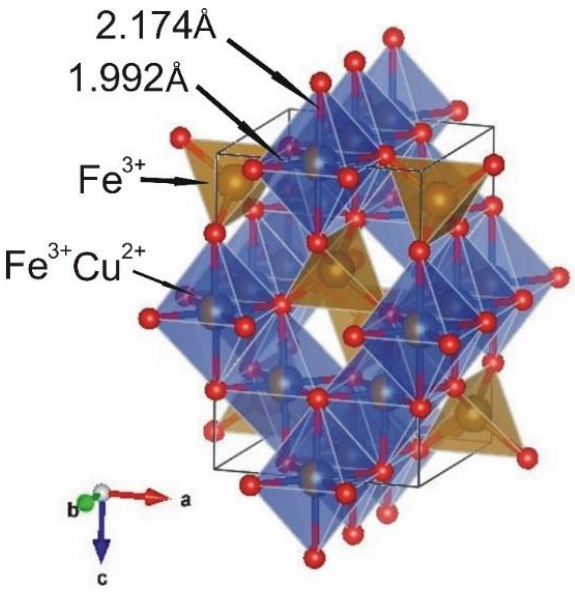

Figure 2. Crystal structure of the tetragonally distorted $CuFe_2O_4$ at ambient conditions.

The structure of copper ferrite can be changed by reducing the copper concentration or alternatively by temperature treatment. Heating can modify the distribution of cations in the spinel lattice - Cu^{2+} ions migrate from octahedral sites to tetragonal positions [18-19]. **Figure 3** shows thermal evolution of the synchrotron X-ray diffraction spinel peaks 311 and 222, in the temperature region of phase transition $F4_1/ddm \rightarrow Fd3m$ for $Cu_{1-x}Ni_xFe_2O_4$ series with x = 0.00, 0.05, 0.1, and 0.15. The temperature dependence of the lattice parameters is also shown in **Fig. 3.** As illustrated in **Fig. 3**, at critical temperatures the axial ratios converge and two phases (tetragonal and cubic) are observed. Phase transition temperature ranges are 390 – 400 ºC for x = 0.00, 330 – 370 ºC for x = 0.05, 210 – 330 ºC for x = 0.1, and 140 – 210 ºC for x = 0.15, respectively. The phase transition result only for $CuFe_2O_4$ has been confirmed in many articles [5,12,20]. The initial phase transition temperature has a linear relationship with the *c/a* ratio (**Fig. 4**). Substitution with Ni^{2+} ions clearly restrains tetragonal distortion effect, decreasing the temperature of structural transformation, and finally stabilizing the cubic structure.

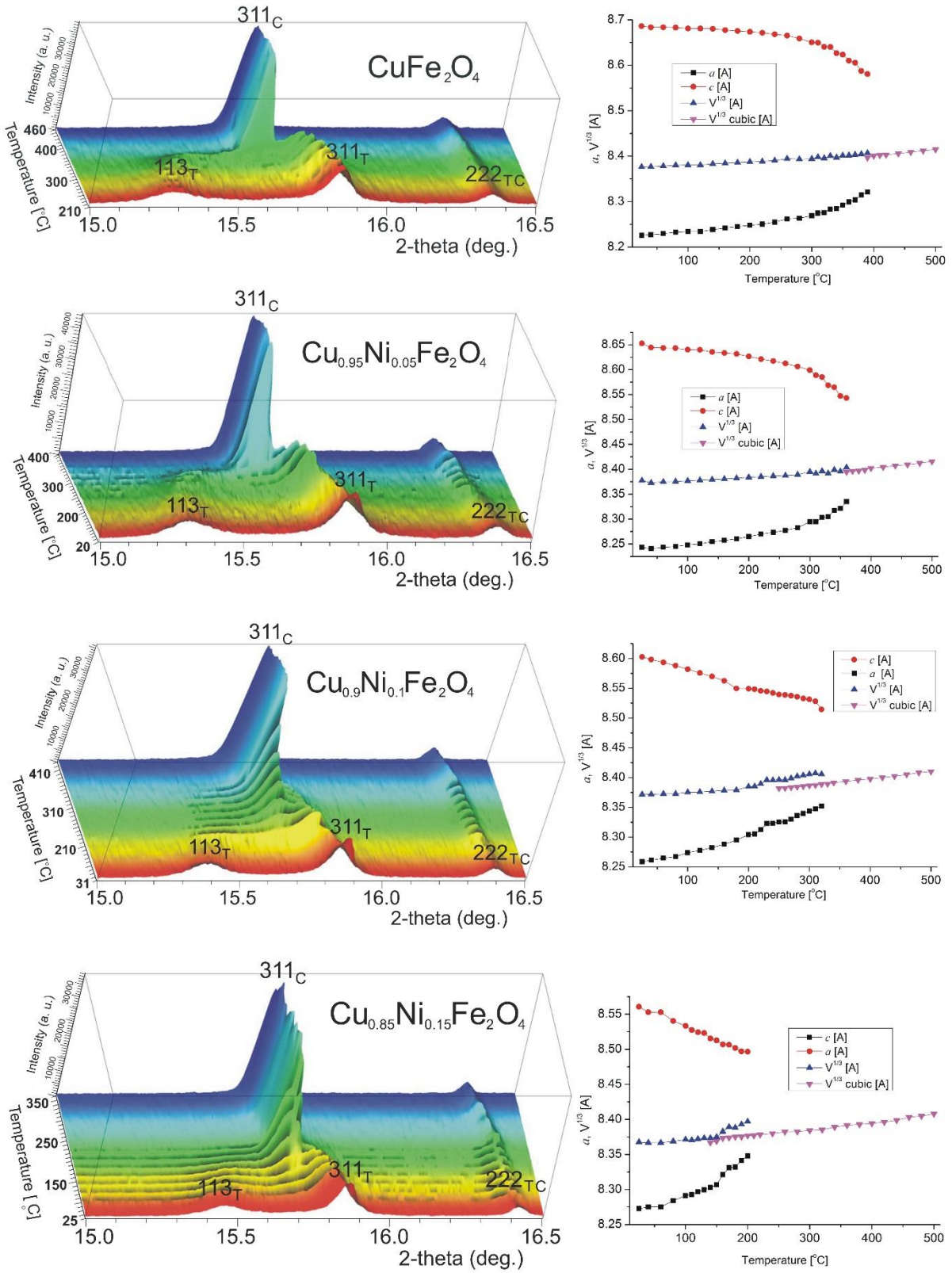

Figure 3. XRD patterns in the temperature region of phase transition from tetragonal to cubic structure for the $Cu_{1-x}Ni_xFe_2O_4$ series. The temperature variation of lattice parameters for $Cu_{1-x}Ni_xFe_2O_4$ compounds. The errors are smaller than the symbols used in the figures.

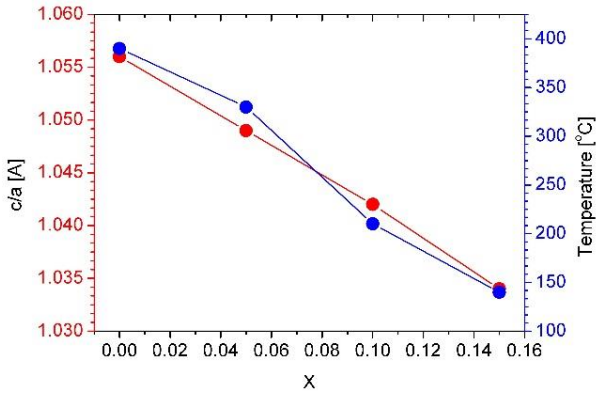

Figure 4. Comparison of the *c/a* ratio with the initial phase transition temperature in the $Cu_{1-x}Ni_xFe_2O_4$ system.

4. Magnetic results

Figures 5a-d show magnetic susceptibility combined of two parts. From 2 K up to 400 K the magnetic susceptibility is obtained by measurements of the temperature dependence of the magnetic moment at magnetic field H = 1 kOe using the QD VSM system. For temperatures up to 850 K the home-made magnetic susceptometer was employed. The VSM results present both the FC and ZFC curves but it should be noted that the splitting of FC - ZFC curves does not have to have a reproducible shape because the upper temperature of 400 K is still much below the magnetic ordering temperature for these ferrites, which is about 780 K [21-23], therefore thermal hysteresis and magnetic history play a role. **Figure 6** presents the normalized high temperature part of magnetic susceptibility for all the studied $Cu_{1-x}Ni_xFe_2O_4$ compositions. While the magnetic ordering temperature changes only slightly with the addition of Ni and takes value in the range 740 - 780 K, the effect of the structural transition is a hump shifting significantly towards lower temperatures with the increase of x (see the vertical lines in **Fig. 6**). The position of the hump is in good agreement with the results of the synchrotron X-ray diffraction experiments (**Fig. 3**). Precise determination of the ordering temperature, T_C, is not possible due to the overlapping of the structural and magnetic phase transitions. For higher Ni concentrations ($x \geq 0.3$) a growth of T_C has been observed previously [6], however it was the temperature dependence of the saturation magnetization, which has been studied, therefore some details observed in our zero-field magnetic susceptibility, like the effect of the structural phase transition, were not visible in Ref. [6]. It is also interesting to follow the behavior of the minimum visible mainly for the FC curves (**Fig. 5**). It may be due to a maximal level of compensation of the magnetic sublattices at those

minima. It then would mean that the Ni addition lowers the temperature, for which the maximal compensation occurs but simultaneously it decreases the level of the compensation.

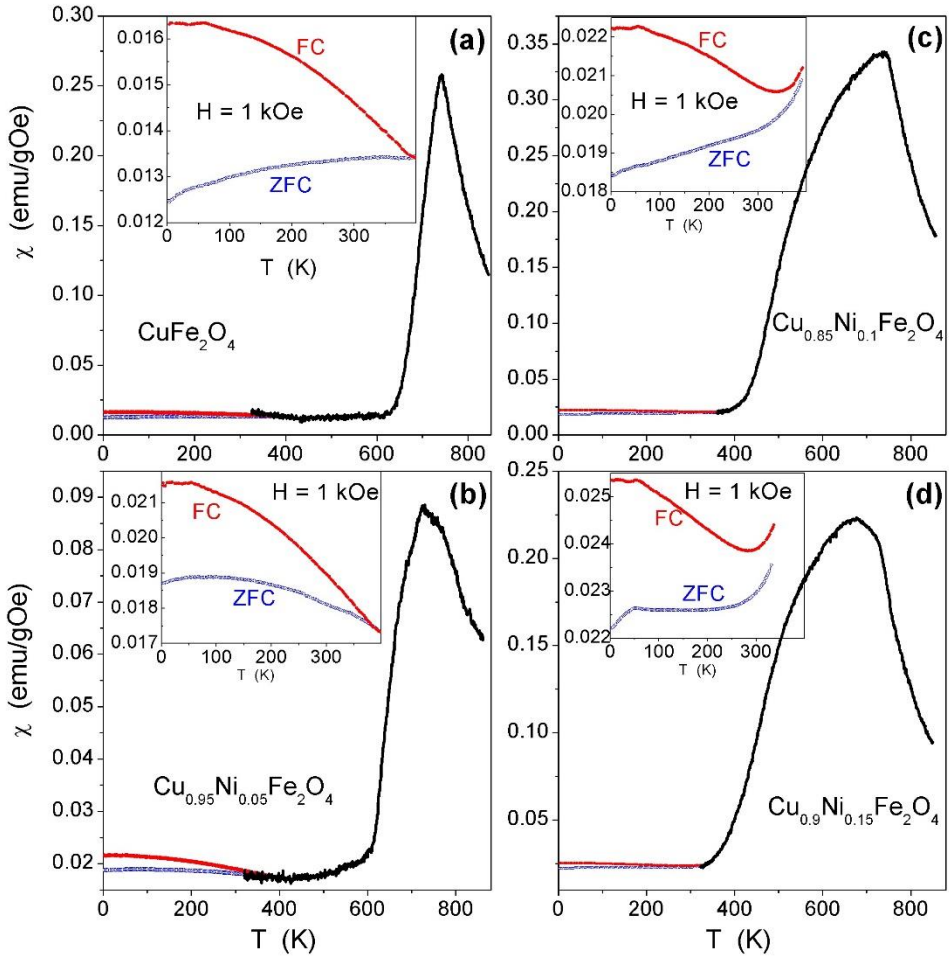

Figure 5. Magnetic susceptibility of the $Cu_{1-x}Ni_xFe_2O_4$ measured with VSM up to 400 K and by a magnetic susceptometer from 300 K up to 850 K.

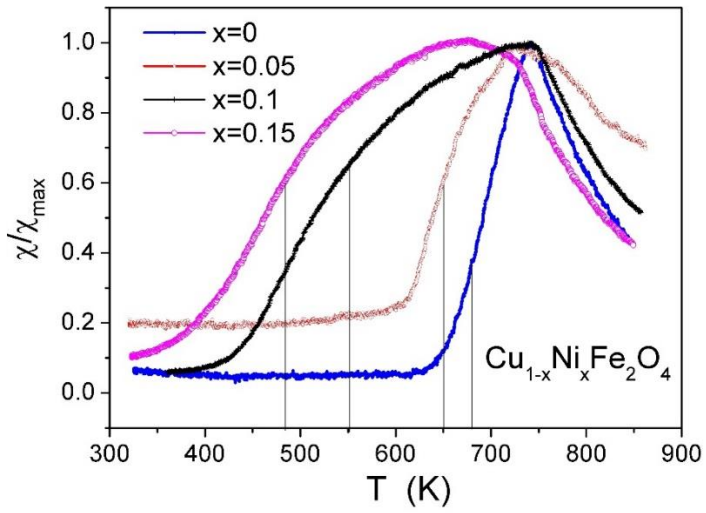

Figure 6. $Cu_{1-x}Ni_xFe_2O_4$: normalized magnetic susceptibility at high temperatures. The vertical lines indicate approximately the initial temperature of the structural phase transition.

The magnetization dependence on magnetic field at temperature of 3 K is gathered in **Fig. 7**. Results including higher temperatures are presented in supplementary Figures S1-S4. The saturation magnetization M_S was determined based on the $M(H)$ data of Fig. 3 and the standard formula describing the magnetic saturation process [24]:

$$M(H) = M_S[1-a/\mu_0 H-b/(\mu_0 H)^2]+cH \quad (3)$$

The values of the parameters of Eq. (1) are collected in **Tab. 2**. **Figure 8** displays the low field part of the $M(H)$ data and reveals a clear hysteresis. The values of the coercive field $\mu_0 H_c$ are also included in **Tab. 2.** Both M_S and $\mu_0 H_c$ are additionally plotted in **Fig. 9** and reveal increasing and decreasing dependence on x, respectively. However, these dependences on Ni content are not perfectly monotonic. In Eq. (3) the parameter b is related to the magnetocrystalline anisotropy and its tendency to decrease with x suggests that the Ni addition decreases the anisotropic properties within the $Cu_{1-x}Ni_xFe_2O_4$ series. It is additionally confirmed by the reduction of the coercive field with increasing x (**Fig. 9**).

Table 2. Magnetic parameters characterizing the $Cu_{1-x}Ni_xFe_2O_4$ series derived from magnetic susceptibility and hysteresis loop measurements.

x	T (K)	M_S (emu/g)	M_S (μ_B)	a (T)	b (T^2)	c (emu/gT)	$\mu_0 H_C$ (T)
0	3	32.08	1.37	0.054	0.043	0	0.070
0	300	27.00	1.16	0.071	0.017	0	0.062
0	350	26.21	1.12	0.042	0.035	0.046	0.056
0.05	3	36.91	1.58	0.025	0.051	0	0.046
0.05	300	32.516	1.39	0.044	0.021	0	0.037
0.05	350	30.72	1.31	0.039	0.019	0.020	0.032
0.1	3	38.08	1.63	0.052	0.027	0	0.045
0.1	300	33.68	1.44	0.041	0.011	0	0.028
0.1	350	31.78	1.36	0.034	0.006	0.013	0.023
0.15	3	42.59	1.82	0.033	0.022	0	0.029
0.15	300	35.94	1.54	0.017	0.011	0.043	0.015
0.15	350	33.53	1.43	0.025	0.002	0.024	0.010

The distribution of cations in all samples was determined, Cu^{2+} and Fe^{3+} ions are distributed in both tetragonal (A) and octahedral [B] sublattices, while Ni^{2+} ions occupy only octahedral [B] sites (**Tab. 3**). The values of magnetic moments at the room temperature determined from magnetization measurements are similar to those obtained from theoretical XRD calculations. Due to the strong preference of Ni^{2+} ions for octahedral sites, it is much easier to design spinels with planned properties and cation distribution.

Table 3. The magnetic moment per unit formula from XRD and VSM data for $Cu_{1-x}Ni_xFe_2O_4$ at the room temperature.

Composition (x)	Cation distribution (XRD)	Magnetic moment [μ_B]	
		Obs. (VSM)	Calc. (XRD)
0.0	$(Cu_{0.03}Fe_{0.97})_A[Cu_{0.97}Fe_{1.03}]_B$	1.16	1.24
0.05	$(Cu_{0.04}Fe_{0.96})_A[Cu_{0.91}Ni_{0.05}Fe_{1.04}]_B$	1.39	1.38
0.1	$(Cu_{0.04}Fe_{0.96})_A[Cu_{0.86}Ni_{0.1}Fe_{1.04}]_B$	1.44	1.44
0.15	$(Cu_{0.04}Fe_{0.96})_A[Cu_{0.81}Ni_{0.15}Fe_{1.04}]_B$	1.54	1.50

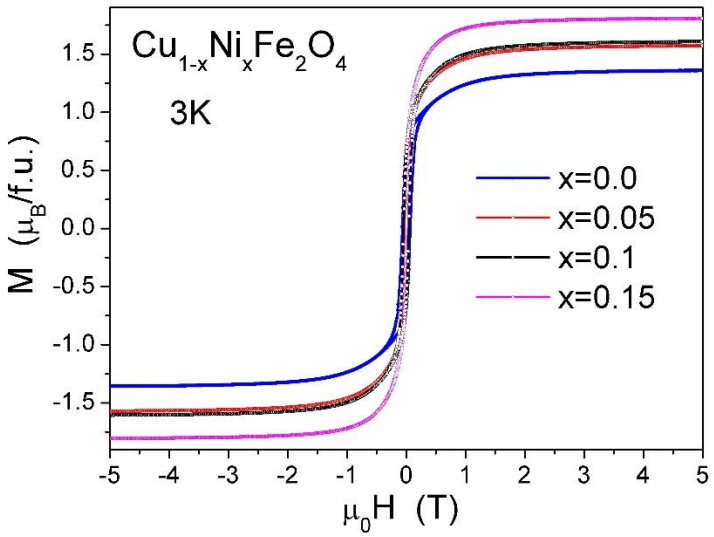

Figure 7. Magnetization curves measured at 3 K for various Ni contents.

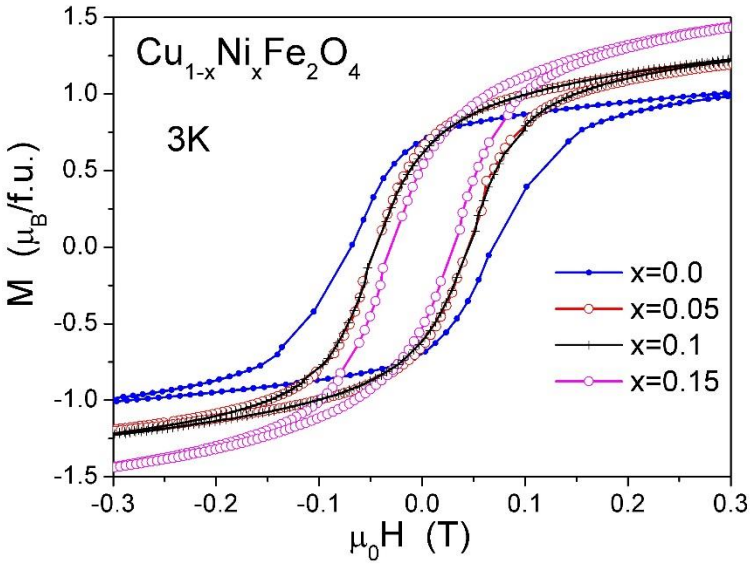

Figure 8. Low magnetic field part of the *M*(*H*) data showing the hysteresis loop.

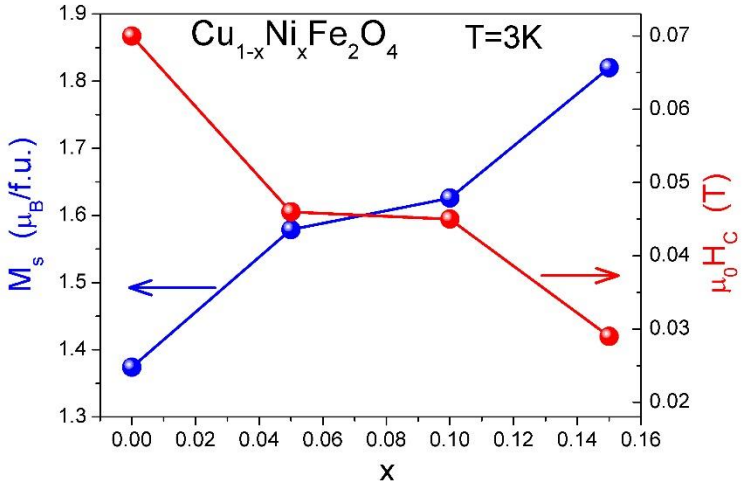

Figure 9. Dependence of the saturation magnetization and the magnetic coercive field on the Ni content in $Cu_{1-x}Ni_xFe_2O_4$.

5. Catalytic activity measurements

Nitrous oxide (N_2O) after carbon dioxide and methane is the third most important greenhouse gas, which has global warming potential is as much as 300 times greater than CO_2 [25]. Spinels are one of the most promising catalytic materials for direct N_2O decomposition [26-29]. Replacing copper with nickel significantly improves the efficiency of N_2O decomposition in the $Cu_{1-x}Ni_xFe_2O_4$ system (**Fig. 10**). The role of Ni can be concluded in the amplification of Cu_{1-x} $Ni_xFe_2O_4$ - structural defects, specific surface and active sites, and thus increasing the catalytic activity of N_2O decomposition. A similar improvement in catalytic activity was observed when nickel was added to cobalt spinel [29].

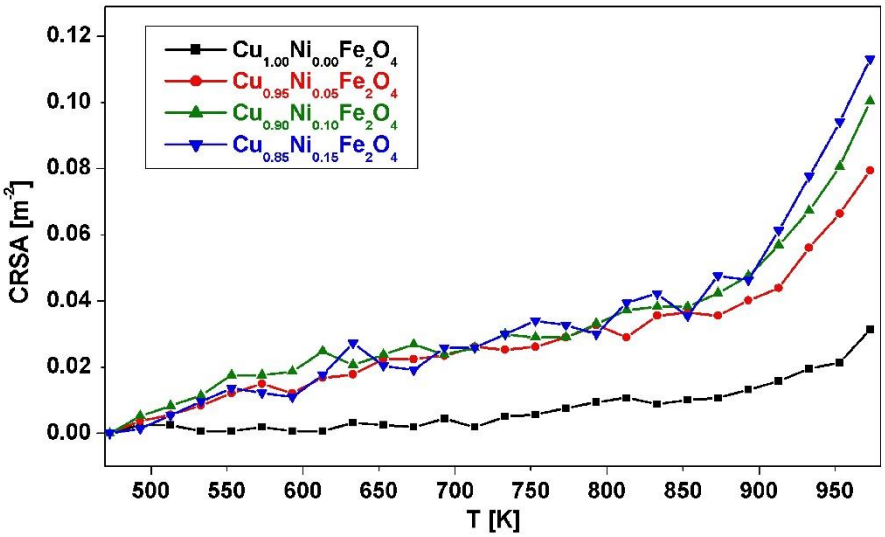

Figure 10. Illustrates N_2O catalytic decomposition curves of $Cu_{1-x}Ni_xFe_2O_4$ samples in conversion rate per square meter of surface area.

6. Conclusions

High-resolution synchrotron powder diffractometer enabled the investigations of the crystallographic structures of the single-phase solid solution series $Cu_{1-x}Ni_xFe_2O_4$ in the very short range ($0 \leq x \leq 0.15$). Substitution with very small quantities of transition ion, restrains the ordering of Cu^{2+} ions occupying the octahedral sites in the spinel lattice and decreases linearly the phase transition temperature. Our results clearly show how we can obtain a new modified material with an optimal cation distribution and well-controlled phase transition temperature. In addition, we modify the magnetic properties and improve the catalytic activity of the thermal decomposition of N_2O.

Ethical approval

The submitted manuscript has not been previously published. Also, no conflict of interest exists in the submission of this manuscript. Furthermore, the manuscript was approved by all authors for publication.

CRediT authorship contribution statement

Zbigniew S. Piskuła: Resources, Supervision, & editing, Writing – original draft, **Jolanta Darul**: Formal analysis, Investigation, **Maria Szafran**: Formal analysis, Investigation of catalytic activity, **Tomasz Toliński**: Formal analysis, Investigation, Writing – original draft., **Waldemar Nowicki**: Conceptualization, Synthesis, Writing – original draft & editing, Formal analysis, Investigation Funding acquisition.

Declaration of Competing Interest

The authors declare that they have no known competing financial interests or personal relationships that could have appeared to influence the work reported in this paper.

Data availability

Data will be made available on request.

Acknowledgments

The synchrotron measurements at Desy-Hasylab were supported by the European Community's Seventh Framework Programme (FP7/2007-2013) under grant agreement no. 226716.

References

[1] S. Anandan, T. Selvamani, G. G. Prasad, A. M. Asiri, J. J. Wu, *Magnetic and catalytic properties of inverse spinel $CuFe_2O_4$ nanoparticles*, J. Magn. Magn. Mater. 432, 437–443 (2017), doi.: 10.1016/j.jmmm.2017.02.026

[2] K. Liua, R. Zhanga, L. Lua, S. B. Mia, M. Liua, H. Wanga, C. L. Jia, *Formation of antiphase boundaries in $CuFe_2O_4$ films induced by rough $MgAl_2O_4$ (001) substrates*, Thin Solid Films, 680, 55-59 (2019), doi: 10.1016/j.tsf.2019.04.020

[3] M. Talaei, S. A. Hassanzadeh-Tabrizi, A. Saffar-Teluri, *Synthesis of mesoporous $CuFe_2O_4$@SiO_2 core-shell nanocomposite for simultaneous drug release and hyperthermia applications*, Ceramics International 47, 30287–30297 (2021), doi: 10.1016/j.ceramint.2021.07.209

[4] W. Liang, W. Yang, S. Sakib, I. Zhitomirsky, *Magnetic $CuFe_2O_4$ Nanoparticles with Pseudocapacitive Properties for Electrical Energy Storage*, Molecules, 27, 5313, (2022), doi: 10.3390/molecules27165313

[4] H. H. Hamdeh, J. C. Ho, S. A. Oliver, R.J. Willey, G. Oliver, G. Busca, *Magnetic properties of partially-inverted zinc ferrite aerogel powders*, J. Appl. Phys. 81,1851 (1997), doi: 10.1063/1.364068

[5] L. G. Antoshina, A. N. Goryaga, E. A. Kamzolov, E. N. Kukudzhanova, On the nature of low-temperature transitions in $CuFe_2O_4$ ferrite, JETP 83, 1149-1151 (1996)

[6] N. K. Thanh, T. T. Loan, L. N. Anh, N. P. Duong, S. Soontaranon, N. Thammajak, T. D. Hien, *Cation distribution in $CuFe_2O_4$ nanoparticles: Effects of Ni doping on magnetic properties*, J. Appl. Phys. 120, 142115 (2016), doi: 10.1063/1.4961722

[7] H. Qin, Y. He, P. Xu, D. Huang, Z. Wang, H. Wang, Z. Wang, Y. Zhao, Q. Tian, Ch. Wang, *Spinel ferrites (MFe_2O_4): Synthesis, improvement and catalytic application in environment and energy field*, Advances in Colloid and Interface Science 294,102486 (2021) doi: 10.1016/j.cis.2021.102486

[8] R. Verma, S. N. Kane, P. Tiwari, S. S. Modak, T. Tatarchuk, F. Mazaleyrat *Ni addition induced modification of structural, magnetic properties and antistructural modeling of $Zn_{1-x}Ni_xFe_2O_4$ (x = 0.0 - 1.0) nanoferrites*, Molecular Crystals and Liquid Crystals, 674:1, 130-141 (2018), doi: 10.1080/15421406.2019.1578519

[9] W. Zhang, A. Sun, X. Zhao, X. Pan, Y. Han, N. Suo, L. Yu, Z. Zuo, *Structural and magnetic properties of Ni - Cu - Co ferrites prepared from sol-gel auto combustion method*

with different complexing agents, J. Alloys Compd. 816, 152501 (2020), doi: 10.1016/j.jallcom.2019.152501

[10] J. Rodriguez-Carvajal, *Recent advances in magnetic structure determination by neutron powder diffraction*, Phys B 192:55–69 (1993), doi: 10.1016/0921-4526(93)90108-I

[11] JCPDS Powder Diffraction File International Centre for Diffraction Data, 12 Campus Boulevard, Newtown Square, PA,USA. 19073-3273

[12] X. X. Tang, A. Manthiram, and J. B. Goodenough, *Copper Ferrite Revisited*, J. Solid State Chem. 79, 250 (1989), doi: 10.1016/0022-4596(89)90272-7

[13] S. Minz, S. C. Sahoo, S. K. Rout, B. Behera, *Structural, temperature/frequency dependence of dielectric, electrical and magnetic properties of Ni-doped inverse spinel $CuFe_2O_4$ nanoferrite*, J. Mater. Sci.: Mater. Electron 34:649 (2023), doi: 0.1007/s10854-022-09791-5

[14] M. Desaia, S. Prasada, N. Venkataramani, I. Samajdar, A. K. Nigamd, R. Krishnane, *Enhanced magnetization in sputter-deposited copper ferrite thin films*, J. Magn. Magn. Mater. 246, 266 (2002), doi: 10.1016/S0304-8853(02)00066-5

[15] H. A. Jahn, E. Teller, *Stability of polyatomic molecules in degenerate electronic states -I-Orbital degeneracy*, Proc. R. Soc. Lond. A161, 220–235 (1937), doi: 10.1098/rspa.1937.0142

[16] P. Jadhav, K. Patankar, V. Mathe, N.L. Tarwal, J.H. Jang, V. Puri, *Structural and magnetic properties of $Ni_{0.8}Co_{0.2-2x}Cu_xMn_xFe_2O_4$ spinel ferrites prepared via solution combustion route*, J. Magn. Magn. Mater. 385, 160–165 (2015), doi.: /10.1016/j.jmmm.2015.03.020

[17] D. R. Patil, B. K. Chougule, *Effect of copper substitution on electrical and magnetic properties of $NiFe_2O_4$ ferrite*, Materials Chemistry and Physics 117, 35–40 (2009), doi:10.1016/j.matchemphys.2008.12.034

[18] W. Nowicki, J. Darul , A.M.T. Bell, *Low temperature structural studies of zinc substituted copper ferrite using synchrotron X-ray powder diffraction*, Z. Kristallogr. Proc. 1 355-360 (2011), doi:10.1524/zkpr.2011.0054

[19] C. Baubet, Ph. Tailhades, C. Bonningue, A. Rousset, Z. Simsa, *Influence of tetragonal distortion on magnetic and magneto-optical properties of copper ferrite films*, J. Phys. Chem. Solids 61, 863–867 (2000), doi: 10.1016/S0022-3697(99)00385-6

[20] J. Darul, W. Nowicki, *Preparation and neutron diffraction study of polycrystalline Cu-Zn-Fe materials*, Rad. Phys. Chem. 78, S109-S111 (2009), doi: 10.1016/j.radphyschem.2009.02.009

[21] B. J. Evans, S. Hafner, *Mössbauer resonance of Fe^{57} in oxidic spinels containing Cu and Fe*, J. Phys. Chem. Solids 29, 1573 (1968), doi: 10.1016/0022-3697(68)90100-5

[22] J. Z. Jiang, G. F. Goya, H. R. Rechenberg, *Magnetic properties of nanostructured $CuFe_2O_4$*, J. Phys.: Condens. Matter 11, 4063 (1999), doi: 10.1088/0953-8984/11/20/313

[23] R. Köferstein, T. Walther, D. Hesse, S. G. Ebbinghaus, *Crystallite growth, phase transition, magnetic properties, and sintering behaviour of nano-$CuFe_2O_4$ powders prepared by a combustion-like process*, Journal of Solid State Chemistry 213, 57 (2014), doi: 10.1016/j.jssc.2014.02.010

[24] S. V. Andreev, M. I. Bartashevich, V. I. Pushkarsky, V. N. Maltsev, L. A. Pamyatnykh, E. N. Tarasov, N. V. Kudrevatykh, T. Goto, J. Alloys Compd. 260, 196 (1997), doi: 10.1016/S0925-8388(97)00127-8

[25] B. Aryal, R. Gurung, A. F. Camargo, G. Fongaro, H. Treichel, B. Mainali, M. J. Angove, H. H. Ngo, W. Guo, S. R. Puadel, *Nitrous oxide emission in altered nitrogen cycle and implications for climate change*, Environmental Pollution, 314, 120272 (2022), doi: 10.1016/j.envpol.2022.120272

[26] M. Konsolakis, *Recent Advances on Nitrous Oxide (N_2O) Decomposition over Non-Noble-Metal Oxide Catalysts: Catalytic Performance, Mechanistic Considerations, and Surface Chemistry Aspects*, ACS Catal., 5, 11, 6397–6421 (2015), doi: 10.1021/acscatal.5b01605

[27] R. Li, Y. Li, Z. Liu, *Recent advances in the catalytic removal of NO_x and N_2O over spinel oxide-based catalyst*, Fuel, 355, 129405 (2024), doi: 10.1016/j.fuel.2023.129405

[28] Z. S. Piskuła, P. Skokowski, T. Toliński, M. Zieliński, P. Kirszensztejn, W. Nowicki, *Structure, magnetic and catalytic properties of SiO_2-MFe_2O_4 (M = Mn, Co, Ni, Cu) nanocomposites and their syntheses by a modified sol–gel method*, Mat. Chem. Phys. 235, 121731 (2019), doi: 10.1016/j.matchemphys.2019.121731

[29] B. M. Abu-Zied, S. A. Soliman, S. E. Abdellah, *Pure and Ni-substituted Co_3O_4 spinel catalysts for direct N_2O decomposition*, Chinese Journal of Catalysis, 35, 7, 1105-1112 (2014), doi:10.1016/S1872-2067(14)60058-9